A Dinuclear Mn^{III}–Cu^{II} Single-Molecule Magnet

Hiroki Oshio,*[a] Masayuki Nihei,[a] Ayano Yoshida,[a] Hiroyuki Nojiri,[b] Motohiro Nakano,*[c] Akira Yamaguchi,[d] Yoshitomo Karaki,[d] and Hidehiko Ishimoto[d]

Abstract: The reaction of 1/3 equivalent of $CuCl_2{\cdot}2H_2O$ with $MnCl_2{\cdot}4H_2O$ and 5-bromo-2-salicylideneamino-1-propanol ($H_2$5-Br-sap) in methanol gave dark brown crystals of [Mn^{III}-Cu^{II}Cl(5-Br-sap)$_2$(MeOH)] (**1**). Complex **1** has an alkoxo-bridged dinuclear core of Mn^{III} and Cu^{II} ions, which have elongated octahedral and square-planar coordination geometries, respectively. In dc magnetic susceptibility measurements, $\chi_m T$ values increased as the temperature was lowered, followed by a sudden decrease below 20 K. This behavior is indicative of the occurrence of intramolecular ferromagnetic interactions, and fitting gave an $S=5/2$ spin ground state with an exchange coupling constant J_{MnCu} of $+78\ cm^{-1}$. Magnetization data collected as a function of temperature and applied magnetic field were analyzed by using a spin Hamiltonian with isotropic Zeeman and axial zero-field splitting (ZFS) terms, and a negative $D_{5/2}$ value ($-1.86\ cm^{-1}$) was obtained. A high-field EPR (HFEPR) spectrum (342.0 GHz) at 4.2 K was composed of four peaks, and two additional peaks at higher magnetic field appeared as the temperature was increased. The temperature dependences in the HFEPR spectra are indicative of a negative $D_{5/2}$ value, and fitting of the data gave $D_{5/2}=-1.81\ cm^{-1}$. In the ac magnetic susceptibility measurements, frequency dependent in-phase (χ_m') and out-of-phase (χ_m'') signals with peak maxima at 0.7–1.5 K were observed and small peaks below 0.7 K appeared. The ac susceptibility data supports that **1** is a single-molecule magnet (SMM). Arrhenius plots for the χ_m'' peaks from 0.7–1.5 K gave the re-orientation energy barrier (ΔE) of 10.5 K with a pre-exponential factor of 8.2×10^{-8} s.

Keywords: copper · magnetic properties · manganese · single-molecule magnets

Introduction

Magnetic relaxation through spin flipping (from up to down spins) along the magnetic anisotropy axis occurs slowly in high-spin molecules with easy axis magnetic anisotropy, and at very low temperature the spin does not thermally flip but flips through quantum processes. Such molecules have a double minimum potential for the reversal direction of the magnetic moment and are called single-molecule magnets (SMMs). SMMs,[1] which have possible applications as very small memory devices, are fundamentally interesting due to quantum phenomena.[2] HFEPR and solid-state NMR spectroscopy have become important tools for studying quantum phenomena in SMMs,[3] and the quantum spin tunnelling and magnetic structures of $[Mn_{12}O_{12}(O_2CMe)_{16}(H_2O)_4]^{n-}$ ($n=0$, 1, and 2)[4] and $[Fe_8O_2(OH)_{12}(tacn)_6]^{8+}$ (tacn = 1,4,7-triazacyclononane)[5] have been extensively studied. To be an SMM, a molecule should have a high-spin ground state with a negative uniaxial zero-field splitting (ZFS) parameter (D). A molecule with the high-spin ground state can be prepared by arranging metal ions orthogonally with respect to their magnetic orbitals.[6] Mn^{III} and Cu^{II} ions, with a dσ hole

[a] Prof. H. Oshio, Dr. M. Nihei, A. Yoshida
Department of Chemistry, University of Tsukuba
Tennodai 1-1-1, Tsukuba 305–8571 (Japan)
Fax:(+81) 298-53-4238
E-mail: oshio@chem.tsukuba.ac.jp

[b] Prof. H. Nojiri
Department of Physics, Okayama University
Tsushimanaka 3-1-1, Okayama 700–8530 (Japan)
Fax: (+81) 86-251-7819
E-mail: nojiri@cc.okayama-u.ac.jp

[c] Prof. M. Nakano
Department of Molecular Chemistry
Graduate School of Engineering
Osaka University, 1-16 Machikaneyama
Toyonaka, Osaka 560–0043 (Japan)
Fax:(+81) 66-850-5570
E-mail: moto@ch.wani.osaka-u.ac.jp

[d] Prof. A. Yamaguchi, Y. Karaki, Prof. H. Ishimoto
Institute for Solid State Physics
The University of Tokyo, Kashiwanoha
Kashiwa 277–8581 (Japan)
Fax:(+81) 471-3522
E-mail: yamagu@issp.u-tokyo.ac.jp

 DOI: 10.1002/chem.200400368

and a dσ unpaired electron, respectively, might be a suitable combination to cause ferromagnetic interactions through strict orthogonality. In the present work, we have prepared a new dinuclear Mn^{III}–Cu^{II} complex using a tridentate Schiff base ligand in which fairly strong ferromagnetic interactions are present. We describe the synthesis, crystal structure, and magnetic properties of the Mn^{III}–Cu^{II} complex, which is a new SMM.

Results and Discussion

Descriptions of structure: The reaction of 1/3 equivalent of $CuCl_2{\cdot}2H_2O$ with $MnCl_2{\cdot}4H_2O$ and Schiff base ligand 5-bromo-2-salicylideneamino-1-propanol ($H_2$5-Br-sap) in methanol gave dark brown crystals of $[Mn^{III}Cu^{II}Cl(5\text{-Br-sap})_2(MeOH)]$ (**1**). Complex **1** crystallizes in the monoclinic space group $P2_1/c$. An ORTEP diagram and projection view on the *bc* plane are shown in Figure 1 and selected bond lengths and angles are listed in Table 1.

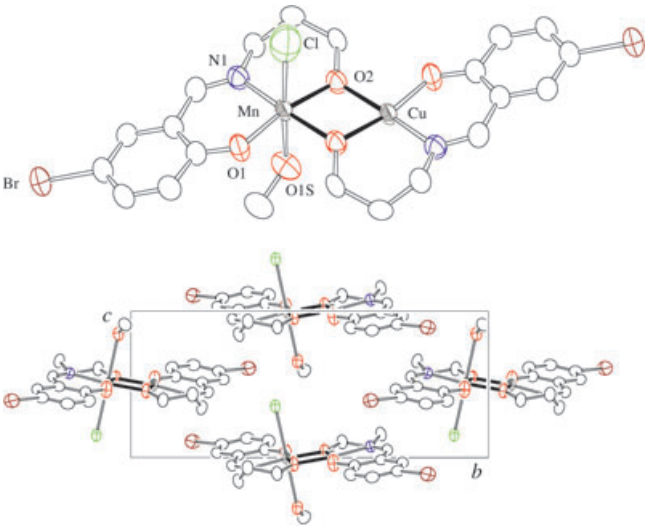

Figure 1. ORTEP diagram (top) and projection view on the *bc* plane (bottom) of **1** with 30% probability. Manganese and copper sites are positionally disordered.

Table 1. Selected interatomic distances [Å] and bond angles [°] for **1**.[a,b]

M–O1	1.880(4)	M–O2	1.913(3)
M–O2#	1.944(4)	M–N1	1.964(4)
Mn–O1S	2.550(8)	Mn–Cl1	2.661(3)
Mn-O2-Cu#	102.1(2)	Mn···Cu#	2.9986(15)

[a] Key to symmetry operation (#): $-x+1, -y+1, -z$. [b] Metal sites are positionally disordered with octahedral Mn^{III} and square-planar Cu^{II} ions, and M represents either Mn or Cu ion.

Complex **1** has a dinuclear structure composed of an Mn^{III} and Cu^{II} core doubly-bridged by two alkoxo groups. The dc magnetic susceptibility data and valence sum considerations support a mixed-metal system and not a 1:1 mixture of homometal system. The dinuclear unit has a crystallographic inversion, and, therefore, the Mn^{III} and Cu^{II} sites are positionally disordered.[7] Each metal ion in the molecule stays on an N_1O_3 coordination plane with a deviation of 0.031(3) Å from the least-squares N_1O_3 plane, and the Mn^{III} and Cu^{II} ions are presumed to have distorted octahedral and square-planar coordination geometry, respectively. It is noted that the possibility of square-pyramidal coordination geometry about the metal ions is ruled out, because metal ions with square-pyramidal coordination geometry are displaced from the equatorial coordination plane. The equatorial positions of the Mn^{III} ion are occupied by three oxygen atoms and one nitrogen atom from the Schiff base ligand with bond lengths in the range of 1.880(4)–1.964(4) Å. The axial positions of the Mn^{III} ion are occupied by a chloride ion and an oxygen atom of the coordinated MeOH and these positions exhibit Jahn–Teller elongation with bond lengths of 2.661(3) (Mn–Cl) and 2.550(8) Å (Mn–O). Coordination bond lengths involving the Cu^{II} ion and the equatorial atoms are the same as those for the corresponding bond lengths of the Mn^{III} ion due to the crystallographic inversion center. The metal ion separation is 3.000(2) Å and the Mn^{III}-O-Cu^{II} angle is 102.1(2)°.

Magnetic properties: The dc magnetic susceptibility measurements for **1** were performed in the temperature range of 1.8–300 K (Figure 2 left). The $\chi_m T$ value at 300 K

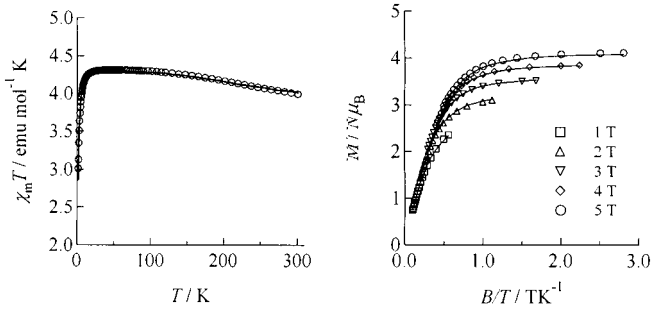

Figure 2. Plots of $\chi_M T$ versus temperature (left) and $M/N\mu_B$ versus B/T (right) for a powder sample of **1**. The solid curves on both plots were fitted using the parameters described in the text.

is 3.92 emu mol^{-1} K, which is larger than the value (3.375 emu mol^{-1} K with $g=2$) expected for uncorrelated Mn^{III} and Cu^{II} ions. The $\chi_m T$ values gradually increased as the temperature was lowered and reached a plateau value (4.20 emu mol^{-1} K) at 100 K, followed by a decrease below 20 K. The plateau value is somewhat smaller than the value of the Curie constant (4.375 emu mol^{-1} K with $g=2$) for an $S=5/2$ state, which is due to the Mn^{III} ion with d^4 configuration, leading to the smaller *g* value of 2.0. Based on temperature-dependent susceptibility data there is substantial ferromagnetic interaction between the Mn^{III} ($S=2$) and Cu^{II} ($S=1/2$) ions. Therefore, the spin ground state *S* equals 5/2. The decrease in the $\chi_m T$ values below 20 K is due to zero-

field splitting and/or intermolecular antiferromagnetic interactions.

Magnetization data for **1** were collected as a function of the temperature and applied magnetic field (Figure 2, right). The $M/N\mu_B$ values did not show saturation up to 5 T, and the magnetic field dependences of the magnetization did not follow the Brillouin function for $S=5/2$. The magnetic susceptibility and low-temperature magnetization data for the powder sample were simultaneously analyzed by using a Heisenberg–Dirac–Van Vleck spin Hamiltonian with intermolecular interactions (zJ') based on a mean field approximation [Eqs. (1)–(5)], in which J_{MnCu} is the intramolecular exchange interaction parameter, D_{Mn} is the uniaxial zero-field splitting parameter for the Mn^{III} ion, g_{Cu} and g_{Mn} are isotropic g factors for Cu^{II} and Mn^{III} ions, respectively, μ_B is the Bohr magneton, and $\boldsymbol{B}$ is the external magnetic field.

$$H = H_{ex} + H_{zfs} + H_{Zeeman} \quad (1)$$

$$H_{ex} = -2J_{MnCu}\boldsymbol{S}_{Mn}\cdot\boldsymbol{S}_{Cu} \quad (2)$$

$$H_{zfs} = D_{Mn}[\boldsymbol{S}_{Z(Mn)}{}^2 - S_{Mn}(S_{Mn}+1)/3] \quad (3)$$

$$H_{Zeeman} = (g_{Cu}\mu_B\boldsymbol{B} - 2zJ' < \boldsymbol{S} >)\cdot\boldsymbol{S}_{Cu} + (g_{Mn}\mu_B\boldsymbol{B} - 2zJ' < \boldsymbol{S} >)\cdot\boldsymbol{S}_{Mn} \quad (4)$$

$$< \boldsymbol{S} >= (g_{Cu} < \boldsymbol{S}_{Cu} > + g_{Mn} < \boldsymbol{S}_{Mn} >)/g_{av} \quad (5)$$

Conventional projection procedures give the relation between the molecular and atomic anisotropy parameters as $D_{5/2}=(16/25)D_{Mn}$.[8] The spin Hamiltonian was solved by iterative diagonalization of a 10×10 matrix followed by a powder average procedure, in which the ground state ($S=5/2$) and the first excited state ($S=3/2$) were included.[9],[10] By using nonlinear least-squares calculations, the best fit parameters J_{MnCu}, $D_{5/2}$, g_{Cu}, g_{Mn}, and zJ' were determined to be $+78\ cm^{-1}$, $-1.86\ cm^{-1}$, 2.095, 1.967, and $-0.01\ cm^{-1}$, respectively. It is noted that a more reliable $D_{5/2}$ value ($-1.81\ cm^{-1}$) was estimated from HFEPR experiments. Simulation curves calculated using these spin Hamiltonian parameters were in good agreement with experimental values (Figure 2).

Under tetragonally elongated octahedral coordination geometry, d orbitals split into e_g (d_{xz} and d_{yz}), b_{2g} (d_{xy}), a_{1g} (d_{z^2}), and b_{1g} ($d_{x^2-y^2}$) orbitals in the order of lower energy. With the square-planar Cu^{II} ion (d^9), an unpaired electron resides in the $d_{x^2-y^2}$ (b_{1g}) orbital, and the Mn^{III} ion (d^4) in the tetragonally elongated octahedral coordination geometry has four spins in the e_g, b_{2g}, and a_{1g} orbitals, which are orthogonal to the b_{1g} orbital of the Cu^{II} ion. This orthogonality of the magnetic orbitals leads to ferromagnetic interactions between the Mn^{III} and Cu^{II} ions.

HFEPR spectra for orientated single crystals, in which the magnetic field was applied along the c axis, were collected at several frequencies (381.5–208.4 GHz) and temperatures. Selected spectra are shown in Figure 3 along with simulated spectra that were generated using estimated parameters.[11] The spectrum at 4.2 K and 342.0 GHz has four peaks at

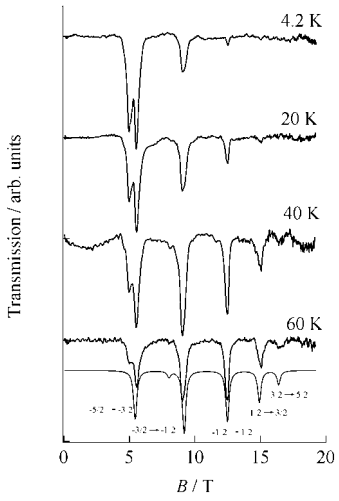

Figure 3. Single-crystal HFEPR spectra (342 GHz) at various temperatures for **1**. The magnetic field was applied along the c axis. The solid curve at the bottom was calculated with $D_{5/2}=-1.81\ cm^{-1}$ and external magnetic field tilted 21.8° away from the magnetic easy axis.

4.97, 5.49, 9.10, and 12.48 T. Two signals with the peak separation of 0.5 T appeared around 5 T. These signals were considered to result from the same origin of the $M_s=-5/2\rightarrow-3/2$ transition, because the peak separation is about ten times larger than the value expected from intermolecular magnetic interactions. The origin of the splitting is not clear, but it might be due to inhomogeneity of the crystal. The resonance at 9.10 T corresponds to $M_s=-3/2\rightarrow-1/2$ transition and that at 12.48 T corresponds to the $M_s=-1/2\rightarrow1/2$ transition. When the temperature was increased from 20 to 60 K, two new peaks, assigned to the $M_s=1/2\rightarrow3/2$ and $3/2\rightarrow5/2$ transitions, appeared at 15.03 and 16.59 T, respectively. When a molecule has a negative D value, the transition at the lowest field becomes the most intense at lower temperature, and more EPR fine structure at higher temperatures is observed at higher magnetic fields. This is due to the appreciable thermal energy required to populate higher energy M_s levels. The temperature dependence of HFEPR measurements indicates that **1** has a negative $D_{5/2}$ value.

The HFEPR spectrum at 342.0 GHz and 60 K was analyzed to obtain a more reliable value of $D_{5/2}$. The spin Hamiltonian used for the HFEPR simulation has the same form as the one used for the powder magnetization analyses except for the Zeeman term, which includes anisotropic g factors and no mean-field contribution [Eqs. (6)–(8)].

$$H_{Zeeman} = \tilde{g}_{Cu}\mu_B\boldsymbol{B}\cdot\boldsymbol{S}_{Cu} + \tilde{g}_{Mn}\mu_B\boldsymbol{B}\cdot\boldsymbol{S}_{Mn} \quad (6)$$

$$\tilde{g}_{Cu} = \begin{bmatrix} g_{Cu}^{\perp} & 0 & 0 \\ 0 & g_{Cu}^{\perp} & 0 \\ 0 & 0 & g_{Cu}^{\parallel} \end{bmatrix} \quad (7)$$

$$\tilde{g}_{Mn} = \begin{bmatrix} g_{Mn}^{\perp} & 0 & 0 \\ 0 & g_{Mn}^{\perp} & 0 \\ 0 & 0 & g_{Mn}^{\parallel} \end{bmatrix} \quad (8)$$

It should be noted that an angle between the principal axis of the magnetic anisotropy tensor and the applied magnetic field was taken into account in the calculation. In a unit cell two molecules are related by a twofold screw axis and each molecule is canted relative to the crystallographic *c* axis (Figure 1, bottom). The external magnetic field for single-crystal HFEPR measurements was applied along with the *c* axis. The angle between the *c* axis and the Mn–Cl bond (Jahn–Teller elongation axis) is 14.28°; however, the principal axis of the magnetic anisotropy tensor on a molecule may slightly differ from the molecular Jahn–Teller axis. Thus the angle θ between the external magnetic field and the anisotropy axis of the molecule was treated as a variable in the fit. Simulation was done by using conventional methods in the references.[8],[11] Simulation curves were evaluated by successive exact diagonalization procedures at every 0.004 T from 0 to 20 T, which was followed by a convolution of Lorentzian shape function. We used well-formed crystals for HFEPR measurements and we obtained excellent quality spectra. The simultaneous optimization of the adjustable parameters (g_{Mn}, g_{Cu}, $D_{5/2}$, θ, and line width) was, therefore, carried out without overparametrization. A least-squares calculation on the HFEPR spectrum recorded at 342.0 GHz and 60.0 K gave the best fit parameters of g_{Mn}, g_{Cu}, $D_{5/2}$, and θ values of 1.994, 2.179, $-1.81\ cm^{-1}$ and 21.8°, respectively.[12] This value of θ is a little larger than the crystallographic tipping angle of 14.28°, but the discrepancy is not significant. The resulting simulation curve is depicted in Figure 3. Figure 4 (top) shows plots of HFEPR frequencies versus observed resonance magnetic fields in the HFEPR spectra. Resonance fields for transitions from an M_s to M_s+1 state can be approximated by the conventional perturbative formula $B_r = h\nu/g\mu_B - (2M_s+1)(3\cos^2\theta-1)D_{5/2}/(2g\mu_B)$;[3a] however, this expression was not sufficient to reproduce the experimental data. Therefore, we used the resonance magnetic fields in 20 simulated EPR spectra with varying frequencies from 200 to 400 GHz and the fixed values of $D_{5/2}$ ($-1.81\ cm^{-1}$) and θ (21.8°). We plotted the resonance magnetic fields versus HFEPR frequencies (solid curves in Figure 4, top). The values were in good agreement with the experimental magnetic resonance fields from the HFEPR spectra over a wide frequency range (381.5–208.4 GHz). The calculated Zeeman splitting of the $S=5/2$ spin ground state under magnetic field tilted 21.8° with respect to the molecular easy axis is shown in Figure 4 (bottom), in which vertical lines correspond to the calculated transitions from M_s to M_s+1 state with $\nu=342.0$ GHz. A small peak at 8 T observed in the spectra of 40 and 60 K was assigned to the $\Delta M_s=2$ transition from $M_s=1/2\rightarrow5/2$ state.

Complex **1** possesses the $S=5/2$ spin ground state with a negative value of $D_{5/2}$, and, therefore, it can be concluded that **1** is an SMM. Thus in complex **1**, magnetic relaxation via spin flipping along the magnetic anisotropy axis should be slow at very low temperature. The ac magnetic susceptibility measurements for aligned single crystals were performed down to 26 mK with a 0.1 mT ac field oscillating at 18.5–618.5 Hz (Figure 5). Both in-phase (χ_m') and out-of-phase (χ_m'') signals were found to be frequency dependent. χ_m' and χ_m'' values increased as the temperature was lowered, reaching the maximum value at 0.7–1.5 K, which was followed by a decrease and the peak maxima shifted to lower temperature region as the ac frequency decreased from 618.5 to 18.5 Hz. The ac susceptibility data supports the conclusion that **1** is an SMM. Small bumps observed below 0.7 K are possibly due to a species with a faster relaxation rate. The analysis of the ac magnetic susceptibility data gives the values of the energy barrier ΔE to reorienta-

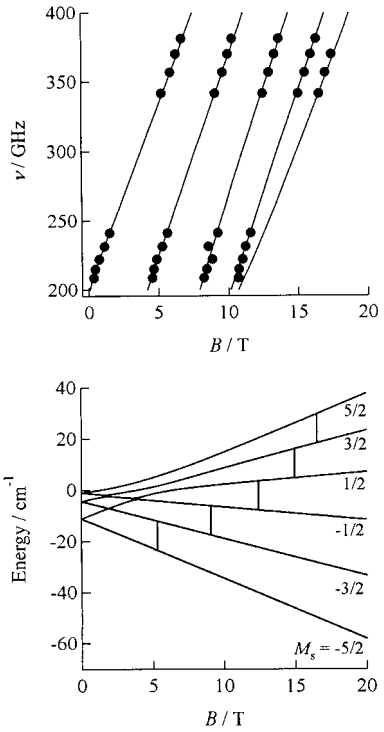

Figure 4. Plots of frequency dependence of resonance field in HFEPR spectra at 60 K (top) and Zeeman splitting of the $S=5/2$ state calculated with $D=-1.81\ cm^{-1}$, $g_{Cu}=2.179$, $g_{Mn}=1.994$, and $\theta=21.8°$ (bottom). Solid curves in the upper diagram were drawn by using resonance magnetic fields in simulating 20 EPR spectra varying frequencies from 200 to 400 GHz and using the above parameters. The vertical lines in lower diagram represent EPR transitions from M_s to M_s+1 state with $\nu=$ 342.0 GHz.

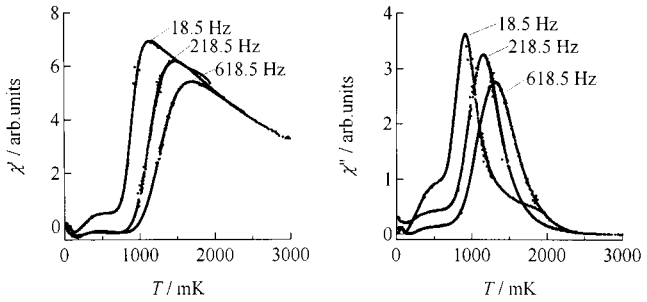

Figure 5. Plots of in-phase (χ_M', left) and out-of-phase (χ_M'', right) ac magnetic susceptibility versus temperature (T) in a 0.1 mT ac field oscillating at the indicated frequencies and with a zero dc field for **1**.

tion between two possible directions of magnetization (M_s = 5/2 and −5/2). Assuming the relaxation time (τ) at the peak-top temperature is well approximated by the inverse of the ac frequency, the Arrhenius plot for the peaks at 0.7–1.5 K gave the ΔE value of 10.5 K with pre-exponential factor of 8.2×10^{-8} s and blocking temperature (T_B) of 0.5 K (Figure 6).

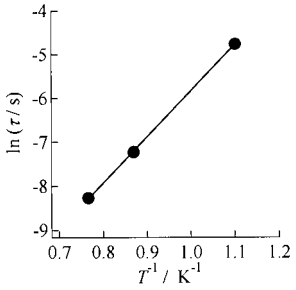

Figure 6. The natural logarithm of the relaxation time (τ) versus the inverse of temperature (T^{-1}) plot for **1**.

Magnetization experiments for oriented single crystals of **1** were performed down to 0.1 K with applying the magnetic field tilted 21.5° with respect to the easy axis (Figure 7).

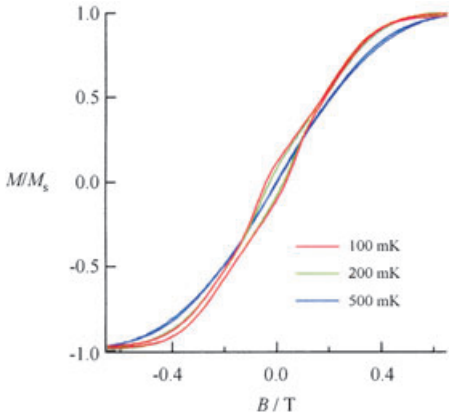

Figure 7. Plots of magnetization (normalized to the saturation magnetization) versus applied magnetic field for **1** at sweep rate of 1.4 mT s^{-1}.

SMMs usually exhibit steplike features in a magnetic hysteresis loop, which are due to a sudden increase in the quantum tunnelling rate at a specific magnetic field. The ac magnetic susceptibility measurements indicated that **1** is an SMM with the T_B of 0.5 K, and preliminary solid-state NMR experiments revealed that no magnetic ordering occurs down to 0.4 K. Hence, complex **1** is expected to show steplike features in the magnetic hysteresis loop below T_B. The plots of magnetization versus external field showed very small coercive fields below 0.2 K. However, the coercivity of the loops did not increase remarkably as the temperature decreased and no steplike features were observed; the reason for this remains unlcear.

Conclusion

A dinuclear Mn^{III}–Cu^{II} SMM containing a bridging tridentate Schiff base ligand was successfully prepared and studied. From dc susceptibility measurements, complex **1** has an $S=5/2$ spin ground state, which is due to substantial ferromagnetic interactions between Mn^{III} and Cu^{II} ions. The ac susceptibility measurements support that **1** is an SMM, and ΔE and T_B values were calculated to be 10.5 K and 0.5 K, respectively. From analysis of both the magnetization and HFEPR data, SMM **1** was shown to have a negative $D_{5/2}$ value (−1.81 cm^{-1}). Tridentate Schiff base ligands are excellent bridging ligands to assemble heterometal ions. Ligand modifications, such as introduction of another alcohol group, and combinations of different metal ions allow for preparation of polynuclear molecules with higher spin ground states.

Experimental Section

Synthesis of [$Mn^{III}Cu^{II}$Cl(5-Br-sap)$_2$(MeOH)] (1): A solution of $MnCl_2\cdot4H_2O$ (198 mg, 1.0 mmol) in methanol (10 mL) was added to a mixture of 5-bromosalicylaldehyde (152 mg, 1.0 mmol), 2-amino-1-ethanol (61 mg, 1.0 mmol), and Et_3N (101 mg, 1.0 mmol), resulting in a dark brown solution, due to air oxidation to Mn^{III} species. $CuCl_2\cdot2H_2O$ (56 mg, 0.33 mmol) in methanol (10 mL) was then added and the mixture was stored for one week. The microcrystalline solid was collected by filtration and recrystallized from methanol to give dark brown crystals of [Mn^{III}-Cu^{II}Cl(5-Br-sap)$_2$(MeOH)] (**1**) in high yield (40%). Elemental analysis calcd (%) for $C_{21}H_{24}Br_2Cl_1Cu_1Mn_1N_2O_5$: C 36.13, H 3.64, N 4.07, Mn 7.87, Cu 9.10; found: C 36.25, H 3.54, N 3.95, Mn 7.52, Cu 8.94.

Physical measurements: Magnetic susceptibility data were collected over a temperature range of 1.8 to 300 K and in an applied field of 500 mT of a Quantum Design model MPMS SQUID magnetometer. Pascal's constants were used to determine the diamagnetic corrections.[13] The ac magnetic susceptibility measurements were performed by using a self-built SQUID magnetometer equipped with a ^{3}He–^{4}He dilution refrigerator. Magnetization measurements below 1.7 K were carried out using a home-made Faraday Force Magnetometer (FFM) installed on a ^{3}He–^{4}He dilution refrigerator. The FFM detects the Faraday force as a change of capacitance between rigid electrode and movable plate on which the sample is mounted. The details of the ac and dc magnetometer are described elsewhere.[12] HFEPR spectra were measured by using a simple transmission method with three types of radiation sources: Gunn oscillators, backward wave oscillators, and a far-infrared laser. An InSb bolometer was used as a detector. A single-shot pulsed field up to 20 T was generated with a capacitor bank of 90 kJ. Details are described elsewhere.[14]

Crystallography: A dark brown crystal ($0.2\times0.2\times0.3$ mm^3) was mounted with epoxy resin on the tip of a glass fiber. Diffraction data were collected at 203 K on a Bruker SMART APEX diffractometer fitted with a CCD-type area detector and a full sphere of data was collected using graphite-monochromated $Mo_{K\alpha}$ radiation ($\lambda=0.71073$ Å). The first 50 frames of data were recollected to establish that the crystal had not deteriorated during data collection.

Data: M_r: 685.54; space group: $P2_1/c$; $a=10.869(2)$, $b=17.733(4)$, $c=7.3442(15)$ Å; $\beta=97.080(4)°$, $V=1404.8(5)$ Å^3, $Z=2$, $T=-70$ °C; $\rho_{calcd}=1.621$ g cm^{-3}; $\mu=43.958$ cm^{-1}; observed data: 6243; $R1$: 0.0495 $wR2=0.1529$; $R1=\Sigma||F_o|-|F_c||/\Sigma|F_o|$. $wR2=[\Sigma[w(F_o^2-F_c^2)^2]/\Sigma[w(F_o^2)^2]]^{0.5}$. Calcd $w=1/[\sigma^2(F_o^2)+(0.1273)^2+0.0000P]$, where $P=(F_o^2+2F_c^2)/3$.

Data frames were integrated by using the SAINT program and were merged to give a unique data set for structure determination. Absorption correction by integration was applied on the basis of measured indexed crystal faces using XPREP, and maximum and minimum transmissions

were 0.76 and 0.44, respectively. A total of 6243 reflections ($2.2° < \theta < 23.3°$) were collected which contained 2021 ($R_{int} = 0.0294$) independent reflections. The structures were solved by direct methods and refined by the full-matrix least-squares method on all F^2 data using the SHELXTL 5.1 package (BRUKER Analytical X-ray Systems). Non-hydrogen atoms were refined with anisotropic thermal parameters. Hydrogen atoms were included in calculated positions and refined with isotropic thermal parameters riding on those of the parent atoms. Full matrix least-squares refinements on F^2 converged to $R1/wR2$ [$I > 2\sigma(I)$] of 0.050/0.15. CCDC-219721 contains the supplementary crystallographic data for this paper. These data can be obtained free of charge from The Cambridge Crystallographic Data Centre via www.ccdc.cam.ac.uk/data_request/cif.

Acknowledgement

This work was partially supported by the COE and TARA projects at the University of Tsukuba and by a Grant-in-Aid for Scientific Research from the Ministry of Education, Science, Sports and Culture, Japan.

[1] a) S. M. J. Aubin, M. W. Wemple, D. M. Adams, H.-L. Tsai, G. Christou, D. N. Hendrickson, *J. Am. Chem. Soc.* **1996**, *118*, 7746; b) S. M. J. Aubin, N. R. Dilley, W. Wemple, M. B. Maple, G. Christou, D. N. Hendrickson, *J. Am. Chem. Soc.* **1998**, *120*, 839; c) C. Boskovic, W. Wernsdorfer, K. Folting, J. C. Huffman, D. N. Hendrickson, G. Christou, *Inorg. Chem.* **2002**, *41*, 5107; d) A. L. Barra, A. Caneschi, D. Gatteschi, R. Sessoli, *J. Am. Chem. Soc.* **1995**, *117*, 8855; e) H. Oshio, N. Hoshino, T. Ito, *J. Am. Chem. Soc.* **2000**, *122*, 12602; f) S. Merlay, T. Mallah, L. Ouahes, P. Veillet, M. Verdaguer, *Inorg. Chem.* **1999**, *38*, 229; g) S. L. Castro, Z. Sun, C. M. Grant, J. C. Bollinger, D. N. Hendrickson, G. Christou, *J. Am. Chem. Soc.* **1998**, *120*, 2365; h) H. Andres, R. Basler, A. J. Blake, C. Cadiou, G. Chaboussant, C. M. Grant, H.-U. Güdel, M. Murrie, S. Parsons, C. Paulsen, F. Semadini, V. Villar, W. Wernsdorfer, R. E. P. Winpenny, *Chem. Eur. J.* **2002**, *8*, 4867; i) E. K. Brechin, M. Soler, J. Davidson, D. N. Hendrickson, S. Parsons, G. Christou, *Chem. Commun.* **2002**, 2252; j) E. K. Brechin, C. Boskovic, W. Wernsdorfer, J. Yoo, A. Yamaguchi, E. C. Sanudo, T. R. Concolino, A. L. Rheingold, H. Ishimoto, D. N. Hendrickson, G. Christou, *J. Am. Chem. Soc.* **2002**, *124*, 9710.

[2] a) M. N. Leuenberger, D. Loss, *Nature* **2001**, *410*, 789; b) D. Gatteschi, R. Sessoli, *Angew. Chem.* **2003**, *115*, 278; *Angew. Chem. Int. Ed.* **2003**, *42*, 268; c) W. Wernsdorfer, N. Aliaga-Alcalde, D. N. Hendrickson, G. Christou, *Nature* **2002**, *416*, 406; d) S. Hill, R. S. Edwards, N. Aliaga-Alcalde, G. Christou, *Science* **2003**, *302*, 1017.

[3] a) S. M. J. Aubin, N. R. Dilley, L. Pardi, J. Krzystek, M. W. Wemple, M. B. Maple, L.-C. Brunel, G. Christou, D. N. Hendrickson, *J. Am. Chem. Soc.* **1998**, *120*, 4991; b) A. L. Barra, D. Gatteschi, R. Sessoli, *Chem. Eur. J.* **2000**, *6*, 1608.

[4] a) A. Caneschi, D. Gatteschi, R. Sessoli, A. L. Barra, L.-C. Brunel, M. Guillot, *J. Am. Chem. Soc.* **1991**, *113*, 5873; b) J. R. Friedman, M. P. Sarachik, J. Tejada, J. Maciejewski, R. Ziolo, *J. Appl. Phys.* **1996**, *79*, 6031; c) H. J. Eppley, H.-L. Tsai, N. De Vries, K. Folting, G. Christou, D. N. Hendrickson, *J. Am. Chem. Soc.* **1995**, *117*, 301; d) M. Soler, W. Wernsdorfer, K. A. Abboud, J. C. Huffman, E. R. Davidson, D. N. Hendrickson, G. Christou, *J. Am. Chem. Soc.* **2003**, *125*, 3576; e) C. Boskovic, M. Pink, J. C. Huffman, D. N. Hendrickson, G. Christou, *J. Am. Chem. Soc.* **2001**, *123*, 9914.

[5] a) D. Gatteschi, R. Sessoli, A. Cornia, *Chem. Commun.* **2000**, 725; b) A. L. Barra, P. Debrunner, D. Gatteschi, C. E. Schulz, R. Sessoli, *Europhys. Lett.* **1996**, *35*, 133; c) Y. Pontilon, A. Caneschi, D. Gatteschi, R. Sessoli, E. Ressouche, J. Schweizer, E. Lelievre-Vera, *J. Am. Chem. Soc.* **1999**, *121*, 5342.

[6] O. Kahn, *Molecular Magnetism*, VCH, Weinheim, **1993**.

[7] In the X-ray analysis the occupancy factors of the chloride ion and coordinated methanol molecule are fixed at 0.5.

[8] A. Benchini, D. Gatteschi, *EPR of Exchange Coupled Systems*, Springer, Berlin, **1990**.

[9] a) G. Armoi, M. J. Knapp, J.-O. Claude, J. C. Huffman, D. N. Hendrickson, G. Christou, *J. Am. Chem. Soc.* **1999**, *121*, 5489; b) H. J. Eppley, H.-L. Tsai, N. de Vries, K. Folting, G. Christou, D. N. Hendrickson, *J. Am. Chem. Soc.* **1995**, *117*, 301.

[10] V. R. Marath, S. Mitra, *Chem. Phys. Lett.* **1974**, *27*, 103.

[11] a) *Handbook of Electron Spin Resonance, Vol. 1* (Eds.: C. P. Poole, H. A. Farach), AIP, New York, **1994**, Chapter II; b) *Handbook of Electron Spin Resonance, Vol. 2* (Eds.: C. P. Poole, H. A, Farach), Springer, New York, **1999**, Chapter IX; c) A. Abragam, B. Bleaney *Electron Paramagnetic Resonance of Transition Ions*, Oxford University Press, Oxford, **1970**.

[12] The contribution of the biaxial anisotropy was ignored in the HFEPR data analysis.

[13] W. E. Hatfield in *Theory and Application of Molecular Paramagnetism* (Eds.: E. A. Boudreaux, L. N. Mulay), Wiley, New York, **1976**, pp. 491–495.

[14] The analysis of ac data for the powdered sample gave a similar ΔE value (10.5 K) and pre-exponential factor (8.9×10^{-8} s).

Received: April 16, 2004
Revised: September 14, 2004
Published online: December 9, 2004